Journal of Electroanalytical Chemistry 823 (2018) 54–60

Contents lists available at ScienceDirect

Journal of Electroanalytical Chemistry

journal homepage: www.elsevier.com/locate/jelechem

Facile synthesis of microporous carbons with three-dimensional honeycomb-like porous structure for high performance supercapacitors

Xin Hu, Xinhao Xu, Renqi Zhong, Lijun Shang, Haotian Ma, Xiaoliang Wu*, Peiyun Jia

Department of Chemistry, College of Science, Northeast Forestry University, 26 Hexing Road, Harbin 150040, PR China

ARTICLE INFO

Keywords:
Microporous carbons
Honeycomb-like porous structure
Energy density
Supercapacitor

ABSTRACT

Microporous carbons (MPC) with three-dimensional (3D) honeycomb-like porous structure is synthesized by a simple and convenient carbonization method using polyvinyl alcohol (PVA) as carbon source and KOH as both activating agent and template. Benefiting from its large surface area, 3D interconnected honeycomb-like porous structure and high oxygen doping, the MPC-2 electrode exhibits a high specific capacitance of 367 F g^{-1} at 0.5 A g^{-1} and excellent electrochemical stability (99.7% of its initial capacitance after 10,000 cycles) in 6.0 M KOH aqueous electrolyte. More importantly, the assembled MPC-2 symmetric supercapacitor shows an energy density of 22.4 Wh kg^{-1} based on the total mass of active materials of the two electrodes in 1.0 M Na_2SO_4 aqueous electrolyte, as well as excellent electrochemical stability. Therefore, this work provides an easy, convenient way to design and large-scale produce 3D honeycomb-like porous carbon for high performance supercapacitors.

1. Introduction

Due to the rapidly increasing market for portable electronic equipment and energy needs, the development of electrochemical energy storage devices has attracted considerable attention [1]. Among energy storage systems, supercapacitors (SCs) have attracted tremendous attention from both industry and academia in recent years, because of their ultrahigh power density, long operating life, fast charge/discharge rate and environmental friendliness [2–6]. Based on the energy storage theory, supercapacitors can be classified into electrical double-layer capacitors (EDLCs) and pseudocapacitors. EDLCs store energy depending on the electrostatic adsorption of electrolyte ions onto the surface of electrode materials, while pseudocapacitors depend on the Faradaic reactions between electrolyte ions and electrode materials. Compared with pseudocapacitors, EDLCs have ultrahigh power density and superior electrochemical stability, which are attributed to the fast reversible adsorption and desorption of electrolyte ions in the double electric layers [7,8].

Carbon-based materials, especially porous carbons (PCs) have been widely used as electrode materials for EDLCs due to their large surface area, low cost, abundance of raw material and excellent mechanical stability [9–15]. It is widely known that the specific surface area and pore size distribution are two critical factors that decide the electrochemical performance of carbon materials [16,17]. Recently, PCs with a well-designed 3D structure have better permeability and can not only provide usable large active surface areas for the interfacial adsorption of ions for different pore sizes, but also shorten diffusion paths and thus favor the fast diffusion of electrolyte ions into the pores, have attracted more and more attention [18–25]. Consequently, a wide range of synthesis routes have been developed for obtaining novel 3D PCs, such as, using expensive zeolites or silica oxides as a sacrificial scaffold [26–28], using a metallic compound as a template [29,30]. However, these ways still suffer from some drawbacks such as complex synthesis processes, costly inorganic templates, which severely limit their application in large-scale production. Therefore, it remains a big challenge for the preparation of 3D interconnected porous carbon with an effective and convenient method.

Herein, we develop a novel, easy strategy to synthesize microporous carbons (MPC) with 3D honeycomb-like porous structure using polyvinyl alcohol (PVA) as the precursor and KOH as both the activating agent and template. The obtained carbon materials process unique 3D interconnected honeycomb-like porous structure, high oxygen doping and large surface area. As a result, the MPC-2 electrode delivers high specific capacitance, good rate performance and electrochemical stability. More importantly, the assembled MPC-2 symmetric supercapacitor exhibits an energy density of 22.4 Wh kg^{-1} based on the total mass of active materials of the two electrodes in 1.0 M Na_2SO_4 electrolyte, as well as good electrochemical stability.

* Corresponding author.
E-mail address: wuxiaoliang90@163.com (X. Wu).

https://doi.org/10.1016/j.jelechem.2018.05.034
Received 19 March 2018; Received in revised form 19 May 2018; Accepted 25 May 2018
Available online 26 May 2018

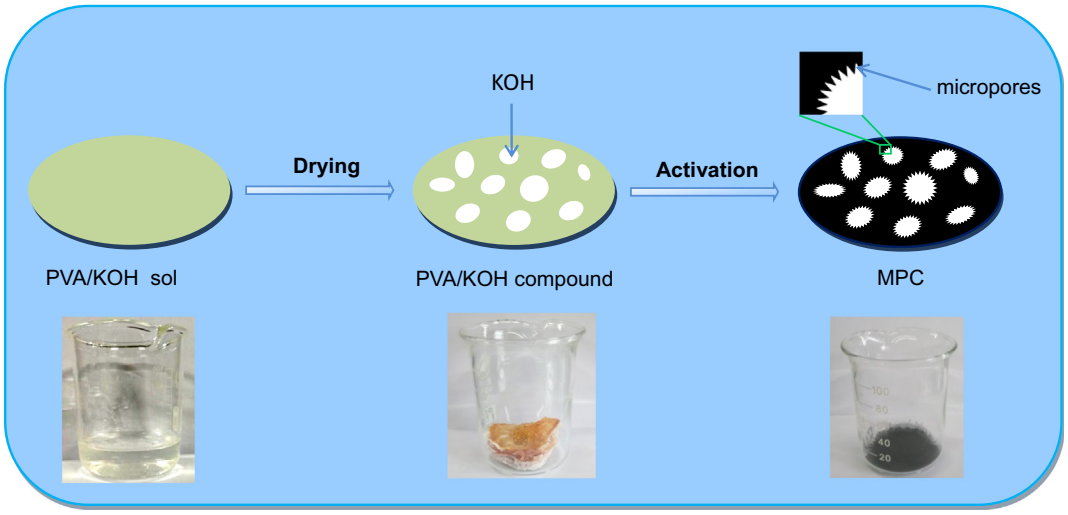

Fig. 1. Schematic diagram of the formation process of MPC.

2. Experimental

2.1. Materials

KOH, polyvinyl alcohol and hydrochloric acid were acquired from Tianjin Yongda Chemical Reagent Co., Ltd. All chemicals and reagents are of analytical grade and were used without any further treatment.

2.2. Preparation of porous carbon materials

KOH (2 g) and polyvinyl alcohol (2 g) were mixed in 30 mL distilled water (85 °C) with stirring until the mixture became limpid. Then, the mixture was dried in a vacuum oven. The resulting product was pyrolyzed in a quartz tube furnace at 700 °C for 2 h under N_2 atmosphere. Then, the obtained example was thoroughly rinsed using dilute hydrochloric acid solution and distilled water several times, and dried in a vacuum oven. For comparison, the different masses of KOH (1 g, 4 g) were also investigated under the above process. The obtained samples were named as MPC-x (which x relates to the mass of KOH). The PVA was directly pyrolyzed at 700 °C for 2 h under N_2 flow, and the obtained example was named as CP. The CP and KOH were mixed with the mass ratio of 1:1, and pyrolyzed at 700 °C for 2 h under N_2 flow, the product was named as ACP. All carbonized samples were rinsed with dilute hydrochloric acid and distilled water several times, and dried in a vacuum oven.

2.3. Material characterizations

The microstructure and morphology of carbon materials were determined by scanning electron microscope (SEM, JEOL JSM-7500F) and transmission electron microscope (TEM, JEOL JEM2010). The crystal structures of carbon materials were checked by X-ray diffraction (XRD) with Cu Kα radiation (λ = 0.15406 nm). Raman analysis was conducted with a Jobin-Yvon HR800 Raman spectroscopy. The surface chemical characteristic of the sample was measured by X-ray photoelectron spectroscopy (XPS) using a PHI5700ESCA spectrometer with a monochromated Al Kα radiation. The specific surface area of samples was tested by N_2 adsorption-desorption isotherms using Barrett-Emmett-Teller (BET) method. The pore size distribution was derived from the adsorption branch of isotherm by density functional theory (DFT) model.

2.4. Electrochemical characterization

Electroactive material, carbon black and poly (tetrafluoroethylene) with a mass ratio of 75:20:5 coated onto the nickel foam current collector (1 cm × 1 cm), and the mass loading was ~3 mg cm^{-2}. The electrochemical measurements of the individual electrode were carried out in 6 M KOH aqueous electrolyte with a three-electrode cell. The prepared electrode acted as the working electrode, platinum foil and Hg/HgO electrode served as counter and reference electrode. The cyclic voltammetry (CV) and galvanostatic charge-discharge tests of the three-electrode system were carried out between −1 and 0 V in 6.0 M KOH aqueous electrolyte. Electrochemical impedance spectra (EIS, Nyquist plots) were evaluated at the frequency range from 100 KHz to 0.01 Hz under an open circuit potential. The symmetric supercapacitor was built using two electrodes with exactly the same mass in 1.0 M Na_2SO_4 aqueous electrolyte, and the electrochemical tests were carried out in a voltage window of 1.8 V. All of the above electrochemical measurements were tested by a CHI 660E electrochemical work station at room temperature.

The specific capacitance (C) was calculated with the following equations:

$$C = \frac{I\Delta t}{m\Delta V} \quad (1)$$

$$C = \frac{\int IdV}{vmV} \quad (2)$$

where I is the response current density, Δt is the discharge time, m is the active mass of the electrode materials. ΔV is the voltage range, and ν is the potential scan rate.

The energy density (E) and power density (P) were calculated based on the following formulas:

$$E = 1/2CV^2 \quad (3)$$

$$P = \frac{E}{t} \quad (4)$$

where t is the discharge time (s).

3. Results and discussion

3.1. Structural characterization

The preparation process of MPC is illustrated in Fig. 1. KOH and polyvinyl alcohol were mixed in 85 °C distilled water with stirring until the mixture became limpid, and then dried in a vacuum oven. The

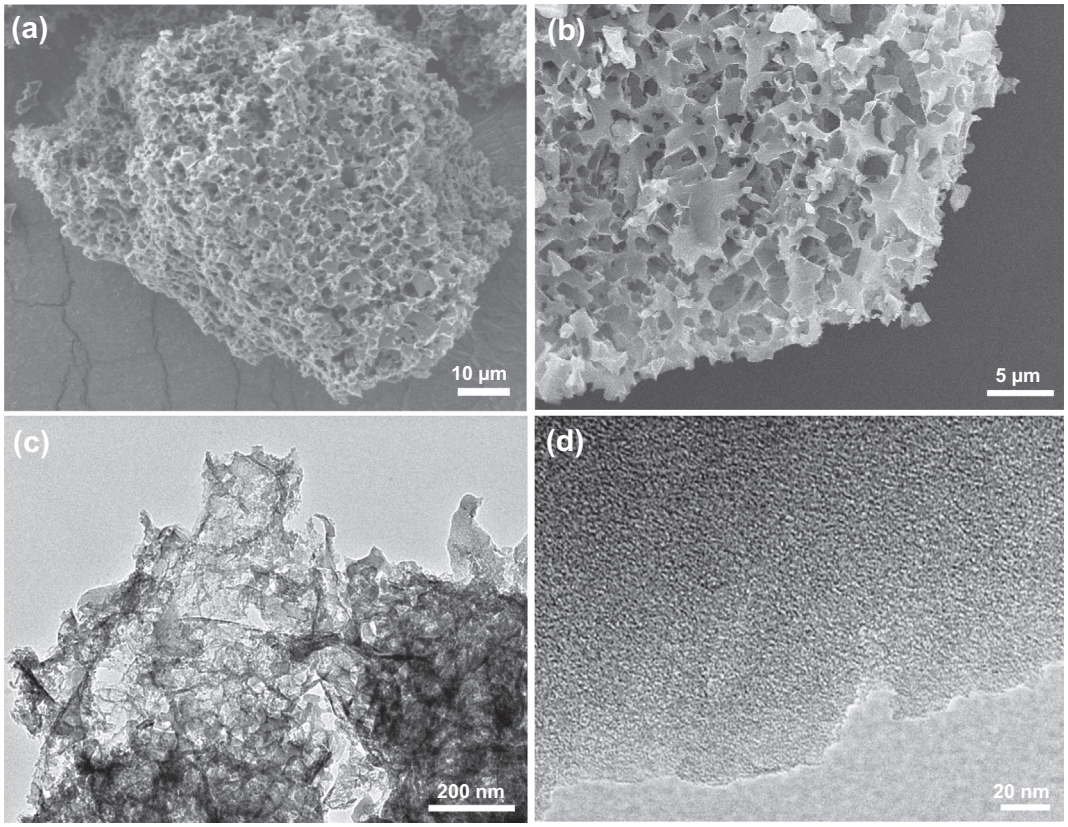

Fig. 2. (a, b) SEM images of MPC-2. (c, d) TEM images of MPC-2.

resulting product was pyrolyzed in a quartz tube furnace at 700 °C for 2 h under N_2 atmosphere. Finally, the obtained products were washed with dilute hydrochloric acid and distilled water to formation of MPC. SEM image of MPC-2 exhibits 3D honeycomb-like porous structure (Fig. 2a). The enlarged resolution SEM image confirms its 3D interconnected porous structure and the void sizes are as large as 1–3 μm (Fig. 2b). Furthermore, the corresponding element mapping images of MPC-2 demonstrate the uniform distribution of C (Fig. S1d), and O (Fig. S1e). TEM images of MPC-2 further confirm its 3D highly interconnected porous architecture and a large number of micropores in the surface of porous carbon (Fig. 1c, d). For comparison, SEM images of direct carbonized PVA (named as CP) (Fig. S1a) and KOH-activated CP (named as ACP) (Fig. S1b) display rather dense bulk structure and the surface exhibit relatively smooth without obvious porous structure. Furthermore, a series of MPCs were synthetized with different KOH/PVA mass ratios. As shown in Fig. S2a and b, all samples have a 3D interconnected honeycomb-like porous structure. With the increasing mass ratio of KOH to PVA, the void sizes of MPC increases correspondingly. The voids sizes of MPC-1 are 0.5–2 μm and the void sizes of MPC-4 increase to 3–5 μm, revealing that the void sizes of MPC can be controlled by adjusting the KOH amount. From the above analysis, it can be inferred that KOH can act as both template and activating agent for the formation of 3D honeycomb-like porous structure and micropores in carbon materials.

The structure characteristics of MPC samples were determined by X-ray powder diffraction (XRD). As shown in Fig. S3a, XRD patterns of all samples exhibit two broad diffraction peaks located at around 23° and 44°, corresponding to the (002) and (101) crystal planes of graphitic carbon, respectively. The intensity of these two peaks is slightly decreased with the increase of KOH, suggesting the presence of more disordered structure [9]. Furthermore, the structure characteristic of MPC-2 was detected by the Raman spectroscopy analysis (Fig. 3a). The D peak located at 1336 cm^{-1} and G peak located at 1576 cm^{-1} are corresponding to the structural defects in the graphitic structure and the inplane vibration of sp^2 carbon atoms, respectively [31–33]. The ratio of the G and D bands (I_G/I_D) of MPC-2 is 1.06, revealing that it is partially graphitized [34]. To evaluate the surface characterization of MPC materials, XPS measurement was carried out, as shown in Fig. S3b. The chemical compositions of all samples are listed in Table 1. The O content of MPC-2 is calculated to be 11.3 at%, which can contribute some pseudocapacitance during the charge/discharge process. In addition, the C1s spectrum of MPC-2 (Fig. S3c) can be fitted to five individual peaks corresponding to sp^2C (284.5 eV), sp^3C (285.6 eV), C—O (286.7 eV), C═O (287.9 eV) and O═C—O (290.3 eV), respectively [35–38]. Furthermore, the pore structure of MPC materials were carried out with the N_2 adsorption-desorption measurement (Fig. 3b). All the examples exhibit the characteristics of type I isotherms. MPC-2 exhibits the Brunauer-Emmett-Teller (BET) specific surface area of 1166 $m^2 g^{-1}$, higher than MPC-1 (760 $m^2 g^{-1}$) and MPC-4 (786 $m^2 g^{-1}$). The pore size distribution of MPC-2 (Fig. S3d) calculated by DFT method exhibits substantial micropores, which is in good agreement with the TEM image. In addition, the micropores are characterized by CO_2 adsorption and desorption isotherm analysis. As shown in Fig. S3e, all the MPC samples have a similar pore size distribution. The pore sizes between approximately 5.5 and 8.0 Å are dominant in all the MPC samples.

3.2. Electrochemical performance

To evaluate the electrochemical performance of the obtained samples, cyclic voltammetry (CV) was first measured by a three-electrode system in 6 M KOH aqueous electrolyte. Fig. 4a shows the CV curves of MPC-1, MPC-2 and MPC-4 measured at a scan rate of 50 mV s^{-1}. All samples exhibit Faradaic humps (Fig. S5b), which confirming capacitive performance both EDLC and pseudocapacitance from oxygen functional groups. In order to further investigate the effect of oxygen functional groups on electrochemical performance, post treated MPC-2

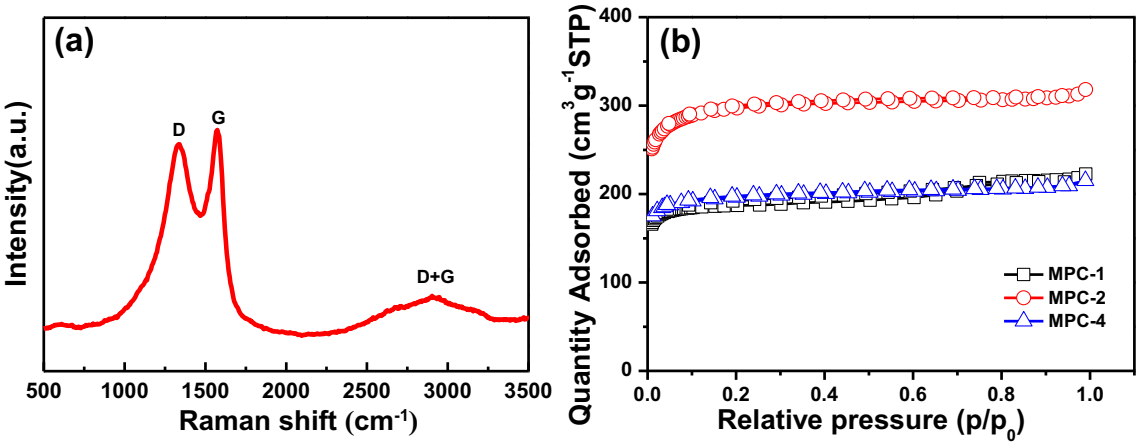

Fig. 3. (a) Raman spectrum of MPC-2. (b) N_2 adsorption/desorption isotherms of MPC-1, MPC-2 and MPC-4.

Table 1
Pore structure parameter and surface elemental compositions of the carbon samples.

Samples	S_{BET} ($m^2 g^{-1}$)[a]	S_{micro}($m^2 g^{-1}$)[b]	V_{total} ($cm^3 g^{-1}$)[c]	Composition (at%)	
				C	O
MPC-1	760	714	0.34	87.8	12.2
MPC-2	1166	1122	0.49	88.7	11.3
MPC-4	786	744	0.33	89.4	10.6

[a] Specific surface area from multiple BET method.
[b] Micropore surface area.
[c] The total pore volume calculated by single adsorption at P/P0 = 0.99.

at 900 °C under N_2 flow (name as MPC-2-900) was measured at a scan rate of 50 mV s^{-1} by CV. Obviously, the MPC-2-900 electrode exhibits a nearly rectangular shape after high-temperature treatment, meaning that the capacitance mainly comes from electric double layer capacitance (Fig. S4b). In addition, the CV curve area of MPC-2 sample is larger than MPC-1 and MPC-4 samples, indicating a higher capacitance for MPC-2. Even at 100 mV s^{-1}, the CV curve of MPC-2 exhibits a quasi-rectangular shape, indicating good capacitive behaviors (Fig. S4a). To further test the electrochemical performance of prepared samples, galvanostatic charge/discharge measurements were measured between −1 to 0 V at different current densities. The galvanostatic charge/discharge curves of the MPC-2 electrode at the current densities of 0.5, 1, 2 and 5 A g^{-1} are shown in Fig. 4b. All the curves exhibit the shape of isosceles triangular, showing that the electrode material has a good capacitive behavior. Moreover, at the current of 5 A g^{-1}, there is no obvious IR drop indicating little internal resistance and good rate performance. As shown in Fig. 4c, the specific capacitance of MPC-2 calculated from the galvanostatic discharge curve is 367 F g^{-1} at 0.5 A g^{-1}, which is higher than commercial activated carbon (YP-50), MPC-1 (277 F g^{-1}) and MPC-4 (326 F g^{-1}). Even at the current densities of 30 A g^{-1}, the MPC-2 electrode still delivers a high specific capacitance of 232 F g^{-1}. In addition, the MPC-2 electrode shows higher specific capacitance than CP, ACP (Fig. S4d) and other previously reported carbon materials (Table 2) [18–22, 28,29, 39–43]. Additionally, we tested the MPC-2 electrode by CV in 1 M Na_2SO_4 aqueous solution using a three-electrode system. The MPC-2 electrode exhibits a nearly rectangular shape in 1 M Na_2SO_4 aqueous solution (Fig. S4c). The specific capacitance of MPC-2 electrode in 6 M KOH electrolyte is higher than that in 1 M Na_2SO_4 electrolyte due to the additional pseudocapacitive charge storage and pore size effects [44].

To investigate the electrode kinetics, Nyquist plots of the carbon materials were measured by electrochemical impedance spectra (Fig. S5). In the high frequency, the MPC-2 sample exhibits a lower equivalent series resistance than others, meaning a faster charge-transfer process for MPC-2. In the low frequency, the MPC-2 electrode shows a nearly vertical line, indicating high electron mobility. The electrochemical stability of the MPC-2 and MPC-2-900 electrodes was investigated at 100 mV s^{-1} for 10,000 cycles. As shown in Fig. 4d, the MPC-2 electrode exhibits the electrochemical stability with 99.6% of its initial capacitance after 10,000 cycles. The MPC-2-900 electrode exhibits ultrahigh electrochemical stability with 100.5% of its initial capacitance after 10,000 cycles, which may be attributed to the increased available active sites during the cycling process (Fig. S5b).

To further evaluate the practical electrochemical performance of the MPC-2 electrode, a symmetric supercapacitor based on two equal MPC-2 electrodes was assembled and investigated in 1 M Na_2SO_4 aqueous electrolyte. As reported by Béguin and Frackowiak, sodium sulfate electrolyte displays a higher decomposition voltage of 2 V than water (~1.2 V) [45,46]. Fig. 5a exhibits the CV profiles of the MPC-2 symmetric supercapacitor tested at 50 mV s^{-1} in different voltage ranges. It can be seen that the CV profiles keep a rectangular-like shape without an obvious increase of anodic current at 1.8 V, meaning the symmetric supercapacitor can be stable tested within the voltage window 0 to 1.8 V. The CV profiles of the symmetric supercapacitor at different scan rates from 20 to 200 mV s^{-1} were shown in Fig. S6. All the profiles display rectangular-like shapes and even at the scan rate of 200 mV s^{-1} without the obvious distortion, indicating good capacitive behavior and rate performance. The symmetric supercapacitor shows a specific capacitance of 49.8 F g^{-1} at the scan rate of 5 mV s^{-1} based on the total mass of electroactive materials on two electrodes (Fig. 5b). Benefitting from its wide working voltage range and large specific capacitance, the MPC-2 symmetric supercapacitor delivers an energy density of 22.4 Wh kg^{-1} (Fig. 5c), higher than most of previously reported carbon-based symmetric supercapacitors in aqueous electrolytes, such as hierarchical porous sandwich-like carbon (18.4 Wh kg^{-1} at 179.9 Wkg^{-1}) [8], hierarchical porous carbon (15.9 Wh kg^{-1} at 317.5 W kg^{-1}) [22], hollow carbon spheres (11.3 Wh kg^{-1} at 127 W kg^{-1}) [47], ordered mesoporous carbon (6.0 Wh kg^{-1} at 1000 W kg^{-1}) [48], and mesoporous carbon (7.8 Wh kg^{-1} at 15 W kg^{-1}) [49]. Additionally, as shown in Fig. 5d, the electrochemical stability of the MPC-2 symmetric supercapacitor was tested at 100 mV s^{-1} for 10,000 cycles and it can remain 97.7% of its initial capacitance, demonstrating excellent electrochemical stability.

The excellent electrochemical performances of MPC-2 can be

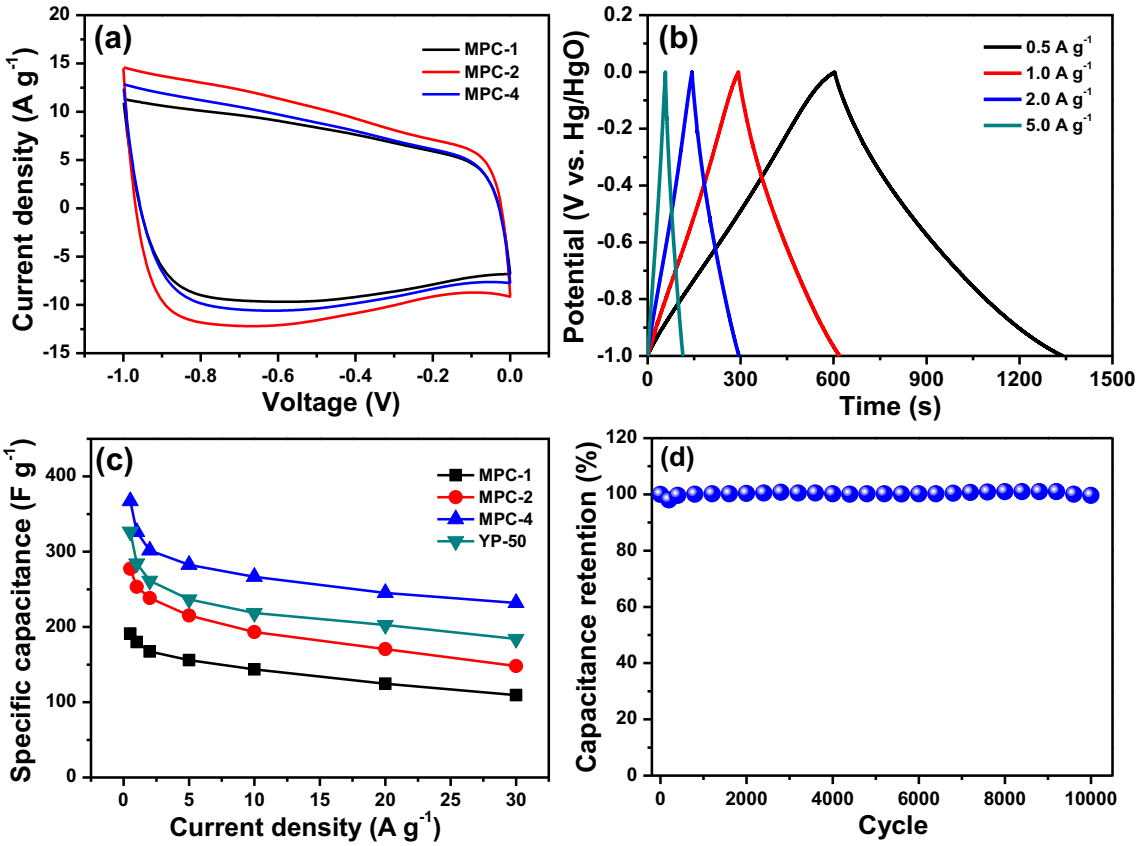

Fig. 4. (a) CV curves of MPC-1, MPC-2 and MPC-4 at the scan rate of 50 mV s^{-1} in 6 M KOH. (b) Galvanostatic charge-discharge profiles of MPC-2 at different current densities of 0.5, 1, 2 and 5 A g^{-1} in 6 M KOH. (c) Specific capacitance of MPC-1, MPC-2, MPC-4 and YP-50 versus current density in 6 M KOH. (d) Specific capacitance of MPC-2 retention versus the number of cycle, tested at 100 mV s^{-1} in 6 M KOH.

Table 2
Summary of electrochemical performance for carbon electrode materials.

Material	C (F g^{-1})	Electrolyte	Ref.
Pitch-derived hierarchical porous carbon	194 (0.1 A g^{-1})	6 M KOH	18
Lignin-derived hierarchical porous carbon	165 (0.05 A g^{-1})	1 M H_2SO_4	19
EDTA-derived hierarchical porous carbon	260 (0. 5 A g^{-1})	6 M KOH	20
Resol-derived hierarchical porous carbon	307 (1.0 A g^{-1})	6 M KOH	21
Pitch-derived hierarchical porous carbon	294 (2.0 mV s^{-1})	6 M KOH	22
Banana peel-derived hierarchical porous carbon	153 (0.5 A g^{-1})	6 M KOH	28
Bagasse-derived hierarchical porous carbon	268 (2.0 mV s^{-1})	6 M KOH	29
Nitrogen-doped hollow carbon spheres	213 (1.0 A g^{-1})	6 M KOH	39
Chicken eggshell membranes derived carbon	297 (1.0 A g^{-1})	1 M KOH	40
Coconut shell sheet-like graphitic carbon	248 (0.5 A g^{-1})	6 M KOH	41
Auricularia derived carbon	196 (5.0 mV s^{-1})	6 M KOH	42
Rice husk derived carbon	112 (1.0 A g^{-1})	1 M Na_2SO_4	43
MPC-2	367 (0.5 A g^{-1})	6 M KOH	This work

attributed to its unique interconnected hierarchical porous structure with large surface area and high level heteroatom doping. Firstly, high specific surface area can offer numerous active sites to store ions and accordingly contribute to large specific capacitance. Secondly, 3D interconnected hierarchical porous structure not only provides a continuous electronic transport channel to ensure fast electron mobility, but also facilitates ion diffuse by shortening diffusion route. Finally, the presence of oxygen containing functional groups can not only improve the surface wettability of porous carbon, but also provide extra pseudocapacitance.

4. Conclusions

In this paper, we have developed a novel, convenient way for the synthesis of 3D hierarchical porous carbon for supercapacitors with polyvinyl alcohol (PVA) as the carbon source and KOH as both the activating agent and template. Benefitting from its interconnected hierarchical porous structure, large surface area and high level heteroatom doping, the MPC-2 electrode exhibits high specific capacitance, good rate capability and excellent electrochemical stability. More importantly, the assembled MPC-2 symmetric supercapacitor

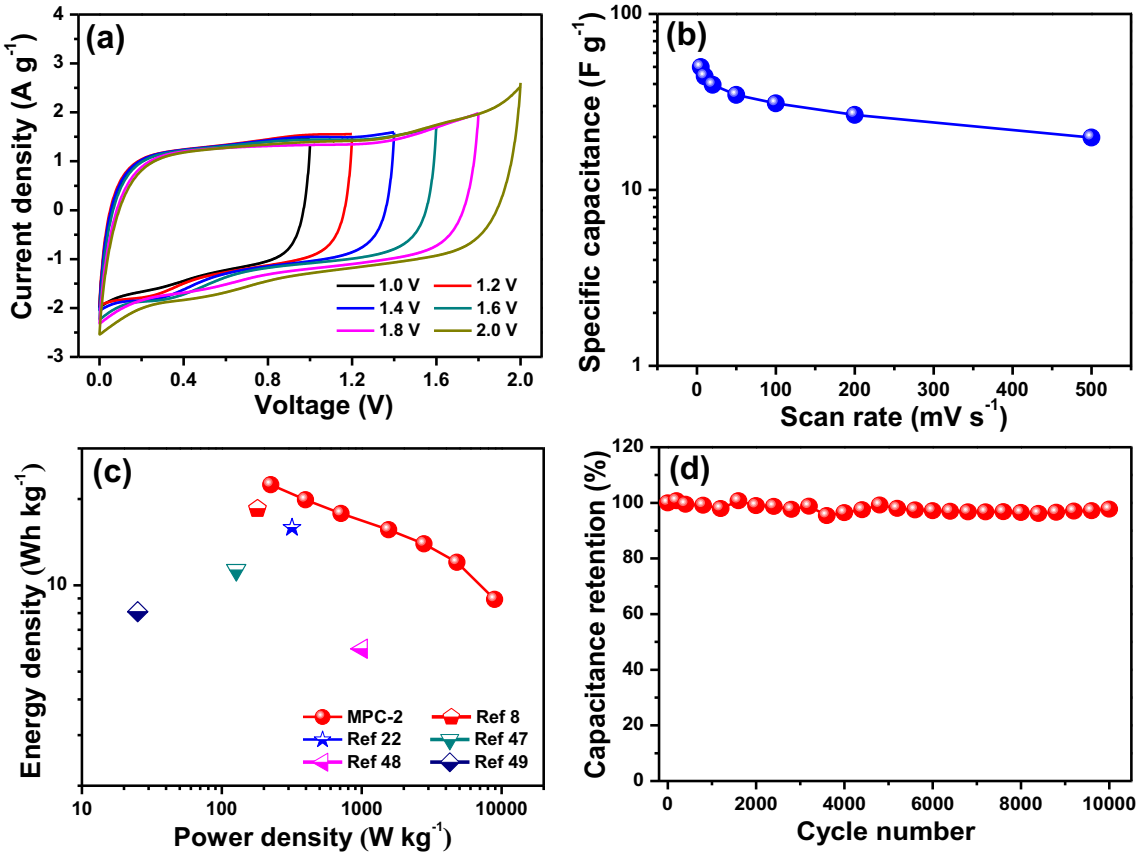

Fig. 5. (a) CV curves of the MPC-2 symmetrical supercapacitor in different operation voltages at the scan rate of 50 mV s^{-1} in 1 M Na_2SO_4. (b) Specific capacitance of the as-assembled MPC-2 symmetrical supercapacitor based on the total mass of the active materials of the two electrodes at different scan rates in 1 M Na_2SO_4. (c) Ragone plots of the MPC-2 symmetrical supercapacitor and other previously reported carbon based symmetric supercapacitors in 1 M Na_2SO_4. (d) Electrochemical stability of the MPC-2 symmetrical supercapacitor for 10,000 cycles tested at 100 mV s^{-1} in 1 M Na_2SO_4.

delivers an energy density of 22.4 Wh kg^{-1} based on the total mass of the active materials of the two Electronic supplementary material:

Acknowledgment

This work was supported by National Natural Science Foundation of China (51702043), Fundamental Research Funds for the Central Universities (2572017BB18) and National Undergraduate Innovative and Entrepreneurial Training Program (201710225043).

Appendix A. Supplementary data

Supplementary data to this article can be found online at https://doi.org/10.1016/j.jelechem.2018.05.034.

References

[1] C. Liu, F. Li, L. Ma, H. Cheng, Advanced materials for energy storage, Adv. Mater. 22 (2010) 28–62.
[2] Q. Wang, J. Yan, Z. Fan, Carbon materials for high volumetric performance supercapacitors: design, progress, challenges and opportunities, Energy Environ. Sci. 9 (2016) 729–762.
[3] L. Liu, Z. Niu, J. Chen, Unconventional supercapacitors from nanocarbon-based electrode materials to device configurations, Chem. Soc. Rev. 45 (2016) 4340–4363.
[4] X. Wu, L. Jiang, C. Long, T. Wei, Z. Fan, Dual support system ensuring porous Co–Al hydroxide nanosheets with ultrahigh rate performance and high energy density for supercapacitors, Adv. Funct. Mater. 25 (2015) 1648–1655.
[5] M. Yu, D. Lin, H. Feng, Y. Zeng, T.X. Ye, X.H. Lu, Boosting the energy density of carbon-based aqueous supercapacitors by optimizing the surface charge, Angew. Chem. Int. Ed. 56 (2017) 1–6.
[6] X.L. Wu, D.R. Yang, C.K. Wang, Y.T. Jiang, T. Wei, Z.J. Fan, Functionalized three-dimensional graphene networks for high performance supercapacitors, Carbon 92 (2015) 26–30.
[7] M. Zhi, C. Xiang, J. Li, M. Li, N. Wu, Nanostructured carbon–metal oxide composite electrodes for supercapacitors: a review, Nano 5 (2013) 72–88.
[8] Y. Li, C. Chen, T. Gao, D. Zhang, X. Huang, Y. Pan, K. Ye, K. Cheng, D. Cao, G. Wang, Synthesis of hierarchically porous sandwich-like carbon materials for high-performance supercapacitors, Chem. Eur. J. 22 (2016) 16863–16871.
[9] X. Wu, L. Jiang, C. Long, Z. Fan, From flour to honeycomb-like carbon foam: carbon makes room for high energy density supercapacitors, Nano Energy 13 (2015) 527–536.
[10] L. Zhang, X. Zhao, Carbon-based materials as supercapacitor electrodes, Chem. Soc. Rev. 38 (2009) 2520–2531.
[11] X. Zheng, J. Luo, W. Lv, D. Wang, Q. Yang, Two-dimensional porous carbon: synthesis and ion-transport properties, Adv. Mater. 27 (2015) 5388–5395.
[12] Z. Li, Z. Xu, H. Wang, J. Ding, B. Zahiri, C. Holt, X. Tan, D. Mitlin, Colossal pseudocapacitance in a high functionality–high surface area carbon anode doubles the energy of an asymmetric supercapacitor, Energy Environ. Sci. 7 (2014) 1708–1718.
[13] Y.S. Yun, M.H. Park, S.J. Hong, M.E. Hong, Y.W. Park, H.J. Jin, Hierarchically porous carbon nanosheets from waste coffee grounds for supercapacitors, ACS Appl. Mater. Interfaces 7 (2015) 3684–3690.
[14] R. Madhu, V. Veeramani, S.S. Chen, A. Manikandan, A.Y. Lo, Y.L. Chueh, Honeycomb-like porous carbon – cobalt oxide nanocomposite for high-performance enzymeless glucose sensor and supercapacitor applications, ACS Appl. Mater. Interfaces 7 (2015) 15812–15820.
[15] S. Liu, S. Sun, X. You, Inorganic nanostructured materials for high performance electrochemical supercapacitors, Nano 6 (2014) 2037–2045.
[16] L. Qie, W. Chen, H. Xu, X. Xiong, Y. Jiang, F. Zou, X. Hu, Y. Xin, Z. Zhang, Y. Huang, Synthesis of functionalized 3D hierarchical porous carbon for high-performance supercapacitors, Energy Environ. Sci. 6 (2013) 2497–2504.
[17] C. Long, X. Chen, L. Jiang, L. Zhi, Z. Fan, Porous layer-stacking carbon derived from in-built template in biomass for high volumetric performance supercapacitors, Nano Energy 12 (2015) 141–151.
[18] K. Sun, S. Yu, Z. Hua, Z. Lia, G. Lei, Q. Xiao, Y. Ding, Oxygen-containing hierarchically porous carbon materials derived from wild jujube pit for high-performance supercapacitor, Electrochim. Acta 231 (2017) 417–428.
[19] W. Zhang, H. Lin, Z. Lin, J. Yin, H. Lu, D. Liu, M. Zhao, 3D hierarchical porous carbon for supercapacitors prepared from lignin through a facile template-free method, ChemSusChem 8 (2015) 2114–2122.
[20] L. Chao, Z. Liu, G. Zhang, X. Song, X. Lei, M. Noyong, U. Simon, Z. Chang, X. Sun,

Enhancement of capacitive deionization capacity of hierarchical porous carbon, J. Mater. Chem. A 3 (2015) 12730–12737.
[21] M. Li, C. Liu, H. Cao, H. Zhao, Y. Zhang, Z. Fan, KOH self-templating synthesis of three-dimensional hierarchical porous carbon materials for high performance supercapacitors, J. Mater. Chem. A 2 (2014) 14844–14851.
[22] Q. Wang, J. Yan, Y. Wang, T. Wei, M. Zhang, X. Jing, Z. Fan, Three-dimensional flower-like and hierarchical porous carbon materials as high-rate performance electrodes for supercapacitors, Carbon 67 (2014) 119–127.
[23] S. Dutta, A. Bhaumik, K. Wu, Hierarchically porous carbon derived from polymers and biomass: effect of interconnected pores on energy applications, Energy Environ. Sci. 7 (2014) 3574–3592.
[24] D. Wang, F. Li, M. Liu, G. Lu, H. Cheng, 3D aperiodic hierarchical porous graphitic carbon material for high-rate electrochemical capacitive energy storage, Angew. Chem. Int. Ed. 47 (2008) 373–376.
[25] Y. Lv, L. Gan, M. Liu, W. Xiong, Z. Xu, D. Zhu, D. Wright, A self-template synthesis of hierarchical porous carbon foams based on banana peel for supercapacitor electrodes, J. Power Sources 209 (2012) 152–157.
[26] Y. Jiao, F. Wang, X. Ma, Q. Tang, K. Wang, Y. Guo, L. Yang, Facile one-step synthesis of porous ceria hollow nanospheres for low temperature CO oxidation, Microporous Mesoporous Mater. 176 (2013) 1–7.
[27] A. Vu, X. Li, J. Phillips, A. Han, W.H. Smyrl, P. Bühlmann, A. Stein, Three-dimensionally ordered mesoporous (3DOm) carbon materials as electrodes for electrochemical double-layer capacitors with ionic liquid electrolytes, Chem. Mater. 25 (2013) 4137–4148.
[28] X. Wen, D. Zhang, T. Yan, J. Zhang, L. Shi, J. Mater. Chem. A 1 (2013) 12334.
[29] K. Xie, X.T. Qin, X.Z. Wang, Y.N. Wang, H.S. Tao, Q. Wu, L.J. Yang, Z. Hu, Adv. Mater. 24 (2012) 347.
[30] X. He, N. Zhao, J. Qiu, N. Xiao, M. Yu, C. Yu, X. Zhang, M. Zheng, Synthesis of hierarchical porous carbons for supercapacitors from coal tar pitch with nano-Fe_2O_3 as template and activation agent coupled with KOH activation, J. Mater. Chem. A 1 (2013) 9440–9448.
[31] S. Stankovich, D. Dikin, R. Piner, K. Kohlhaas, A. Kleinhammes, Y. Jia, Y. Wu, S. Nguyen, R. Ruoff, Synthesis of graphene-based nanosheets via chemical reduction of exfoliated graphite oxide, Carbon 45 (2007) 1558–1565.
[32] Z. Lin, G. Waller, Y. Liu, M. Liu, C. Wong, Facile synthesis of nitrogen-doped graphene via pyrolysis of graphene oxide and urea, and its electrocatalytic activity toward the oxygen-reduction reaction, Adv. Energy Mater. 2 (2012) 884–888.
[33] A. Ferrari, J. Robertson, Interpretation of Raman spectra of disordered and amorphous carbon, Phys. Rev. B 61 (2000) 14095–14107.
[34] H. Wang, Z. Xu, A. Kohandehghan, Z. Li, K. Cui, X. Tan, T.J. Stephenson, C.K. King'ondu, C.M.B. Holt, B.C. Olsen, J.K. Tak, D. Harfield, A.O. Anyia, D. Mitlin, Interconnected carbon nanosheets derived from hemp for ultrafast supercapacitors with high energy, ACS Nano 7 (2013) 5131–5141.
[35] J. Yan, Q. Wang, T. Wei, L. Jiang, M. Zhang, X. Jing, Z. Fan, Template-assisted low temperature synthesis of functionalized graphene for ultrahigh volumetric performance supercapacitors, ACS Nano 8 (2014) 4720–4729.
[36] Y. Fang, B. Luo, Y. Jia, X. Li, B. Wang, Q. Song, F. Kang, L. Zhi, Renewing functionalized graphene as electrodes for high-performance supercapacitors, Adv. Mater. 24 (2012) 6348–6355.
[37] Z. Fan, W. Kai, J. Yan, T. Wei, L. Zhi, J. Feng, Y. Ren, L. Song, F. Wei, Facile synthesis of graphene nanosheets via Fe reduction of exfoliated graphite oxide, ACS Nano 5 (2011) 191–198.
[38] S. Park, J.H. An, R.D. Piner, I. Jung, D.X. Yang, A. Velamakanni, S.T. Nguyen, R.S. Ruoff, Aqueous suspension and characterization of chemically modified graphene sheets, Chem. Mater. 20 (2008) 6592–6594.
[39] J. Han, G. Xu, B. Ding, J. Pan, H. Dou, D.R. Macfarlane, Porous nitrogen-doped hollow carbon spheres derived from polyaniline for high performance supercapacitors, J. Mater. Chem. A 2 (2014) 5352–5357.
[40] Z. Li, L. Zhang, B.S. Amirkhiz, X. Tan, Z. Xu, H. Wang, B.C. Olsen, C.M.B. Holt, D. Mitlin, Carbonized chicken eggshell membranes with 3D architectures as high-performance electrode materials for supercapacitors, Adv. Energy Mater. 2 (2012) 431–437.
[41] L. Sun, C. Tian, M. Li, X. Meng, L. Wang, R. Wang, J. Yin, H. Fu, From coconut shell to porous graphene-like nanosheets for high-power supercapacitors, J. Mater. Chem. A 1 (2013) 6462–6470.
[42] H. Zhu, X. Wang, F. Yang, X. Yang, Promising carbons for supercapacitors derived from fungi, Adv. Mater. 23 (2011) 2745–2748.
[43] A. Ganesan, R. Mukherjee, J. Raj, M. Shaijumon, Nanoporous rice husk derived carbon for gas storage and high performance electrochemical energy storage, J. Porous. Mater. 21 (2014) 839–847.
[44] Y.S. Yun, S. Lee, N.R. Kim, M. Kang, C. Leal, K.Y. Park, K. Kang, H.J. Jin, High and rapid alkali cation storage in ultramicroporous carbonaceous materials, J. Power Sources 313 (2016) 142–151.
[45] M. Bichat, E. Raymundo-Piñero, F. Béguin, High voltage supercapacitor built with seaweed carbons in neutral aqueous electrolyte, Carbon 48 (2010) 4351–4361.
[46] M. He, K. Fic, E. Frackowiak, P. Novak, E. Berg, Ageing phenomena in high-voltage aqueous supercapacitors investigated by in situ gas analysis, Energy Environ. Sci. 9 (2016) 623–633.
[47] Q. Wang, J. Yan, Y. Wang, G. Ning, Z. Fan, T. Wei, J. Cheng, M. Zhang, X. Jing, Template synthesis of hollow carbon spheres anchored on carbon nanotubes for high rate performance supercapacitors, Carbon 52 (2013) 209–213.
[48] W. Xing, S. Qiao, R. Ding, F. Li, G. Lu, Z. Yan, H. Cheng, Superior electric double layer capacitors using ordered mesoporous carbons, Carbon 44 (2006) 216–224.
[49] X. He, R. Li, J. Qiu, K. Xie, P. Ling, M. Yu, X. Zhang, M. Zheng, Synthesis of mesoporous carbons for supercapacitors from coal tar pitch by coupling microwave-assisted KOH activation with a MgO template, Carbon 50 (2012) 4911–4921.